REVIEW

Quantitative analysis of fetal magnetic resonance phantoms and recommendations for an anthropomorphic motion phantom

Michael Shulman[1,2] · Eunyoung Cho[1,2] · Bipin Aasi[1,2] · Jin Cheng[1,2] · Saiee Nithiyanantham[1,2] · Nicole Waddell[1,2] · Dafna Sussman[1,2,3,4]

Abstract

Objective To provide a review and quantitative analysis of the available fetal MR imaging phantoms.

Materials and methods A literature search was conducted across Pubmed, Google Scholar, and Ryerson University Library databases to identify fetal MR imaging phantoms. Phantoms were graded on a semi-quantitative scale in regards to four evaluation categories: (1) anatomical accuracy in size and shape, (2) dielectric conductivity similar to the simulated tissue, (3) relaxation times similar to simulated tissue, and (4) physiological motion similar to fetal gross body, cardiovascular, and breathing motion. This was followed by statistical analysis to identify significant findings.

Results Seventeen fetal phantoms were identified and had an average overall percentage accuracy of 26%, with anatomical accuracy being satisfied the most (56%) and physiological motion the least (7%). Phantoms constructed using 3D printing were significantly more accurate than conventionally constructed phantoms.

Discussion Currently available fetal phantoms lack accuracy and motion simulation. 3D printing may lead to higher accuracy compared with traditional manufacturing. Future research needs to focus on properly simulating both fetal anatomy and physiological motion to produce a phantom that is appropriate for fetal MRI sequence development and optimization.

Keywords Fetus · Magnetic Resonance Imaging · Phantoms · Imaging · Artifacts · Accuracy assessment · 3D printing · Synthesis methods

Introduction

Background

Magnetic Resonance Imaging (MRI) is an invaluable diagnostic tool that complements ultrasound in obstetric settings by providing non-invasive, high-contrast, multi-planar, 3-dimensional imaging of fetal anatomy [1, 2]. The primary disadvantage of fetal MRI is that its image quality is easily degraded by Motion Artifacts (MAs) which primarily result from spontaneous gross fetal movement during image acquisition, and to a lesser extent from maternal motion, including breathing and bowel motion [1, 3–8]. While shortening the acquisition time can partially address this challenge, this approach at the same time restricts the spatial resolution and image contrast, leading to a lower image quality [8]. An alternative approach has been to develop MR pulse sequences that account for fetal motion and to remove motion effects during image post-processing (for example: [9–11]).

Development and testing of these pulse sequences necessitate the use of motion phantoms [12, 13]. However, these phantoms commonly have a very rudimentary design that does not simulate the complex and dynamic anatomy of the gravid uterus [14], which is often accompanied by unique tissue-related artifacts [5]. While the use of pregnant animals could address this need, the repeated and extended sequence

✉ Dafna Sussman
  dafna.sussman@ryerson.ca

1 Department of Electrical, Computer, and Biomedical Engineering, Ryerson University, Toronto, ON M5B 2K3, Canada

2 Institute for Biomedical Engineering, Science and Technology (iBEST), Ryerson University and St. Michael's Hospital, Toronto, ON M5B 1T8, Canada

3 The Keenan Research Centre for Biomedical Science, St. Michael's Hospital, Toronto, ON M5B 1T8, Canada

4 Department of Biomedical Physics, Ryerson University, Toronto, ON M5B 2K3, Canada

testing on animals is time-consuming, expensive, and necessarily inaccurate because of the required use of sedation which inhibits fetal motion and is not representative of the human scenario [12]. Use of a single MRI phantom that is anthropomorphic but that also simulates fetal motion would permit faster and more accurate testing with reproducible and accurate images [12, 15]. Thus, a fetal Anthropomorphic MR Motion Phantom (AMP) could shorten the sequence development time, accelerate the clinical translation of new sequences, and enhance the diagnostic quality of fetal MR imaging.

While maternal and fetal motion can be controlled to some degree with breath holds or sedation, even minor spontaneous gross fetal movements as well as fetal cardiovascular and respiratory motion can significantly degrade MR image quality [1, 16–19]. Fetal cardiovascular movement begins at the end of 4 weeks of gestation and increases from 110 Beats Per Minute (BPM) to 170 BPM at 9 weeks [20]. The heart rate then gradually decreases until term, when the mean heart rate is 135 BPM [21]. Fetal breathing motion is a complex phenomenon consisting of rhythmic movement of the fetal chest and abdominal wall [22]. Mean Gestational Age (GA) at the onset of abdominal movement is at 18 ± 2 weeks, while the onset of chest movement is at 21 ± 3 weeks [23]. The average fetal respiratory rate is 44 breaths/min at 24–28 weeks and 43 breaths/min at 28–39 weeks [22, 24]. The onset of gross fetal motion, characterized by trunk movement, occurs at 7.5–8.5 weeks and continues until delivery [25, 26]. The mean number of gross fetal body movements at 22–34 weeks is 60 movements/h, which then gradually decreases to an average of 40 movements/h from 35 weeks to term [27, 28]. The gradual decrease in movement frequency as the fetus grows is generally attributed to a decrease in intrauterine space as well as the establishment of behaviour states after 30 weeks [29].

The purpose of this study was to identify and quantitatively analyze all fetal MRI phantoms that have been published to date. A narrative review to identify published phantoms was followed by a quantitative analysis of each phantom's accuracy based on chosen evaluation criteria. Then, a secondary narrative review was conducted to draw conclusions from the data and provide recommendations on how to construct an ideal fetal AMP. We aimed to provide a valuable reference for researchers who plan to build or use a fetal MRI phantom and will demonstrate the importance of integrating AMPs in fetal MR studies.

Methods

Data source and search strategy for phantom identification

A literature search was conducted using PubMed, Google Scholar, and Ryerson University Library (RUL) databases to identify all fetal MRI phantoms published prior to April 6th, 2019. In an initial search on PubMed and RUL databases, the search term 'fetal MRI phantom' was used. This was followed by a secondary search using the following keywords: ('fetus' or 'fetal') AND ('MRI' or 'Magnetic Resonance Imaging') AND ('phantom' or 'anthropomorphic phantom' or 'model' or 'in vitro model' or 'physical model') AND ('pregnant woman' or 'gravid abdomen' or 'pregnant abdomen' or 'heart' or 'lungs' or 'brain' or 'liver' or 'placenta' or 'placental' or 'amniotic fluid' or 'artificial amniotic fluid' or 'gravid uterus') NOT ('mouse' or 'sheep' or 'rat' or 'rabbit' or 'primate' or 'porcine'). For every search conducted on the RUL database, the option to 'add results beyond library collection' was used to widen the search. Both primary and secondary searches examined only articles with these keywords in the abstract to ensure that only relevant articles were reviewed.

The searched keywords in Google Scholar had to be modified because this search engine displays articles that are in a similar research area to the keywords used, regardless if they contain them in their full-text. The searches that were conducted on Google Scholar and the respective number of article titles that were reviewed were as follows: 'fetal MRI phantom' (first 50 articles), 'anthropomorphic fetal MRI phantom' (first 50 articles), and 'MRI phantom of fetus' (first 100 articles). The results were further limited to articles published between 2005 and 2019 primarily due to the unlikelihood of fetal MRI phantom development prior to 2005.

Inclusion and exclusion criteria

Articles were included in the narrative review only if they reported on the use or development of a fetal MRI phantom. A fetal MRI phantom was defined as an artificial physical model that either simulates the human gravid uterus, fetal organs, or maternal body parts and which has undergone MR imaging. Non-English articles, non-MRI studies without the conjunction of MRI, non-(fetal or phantom) studies, as well as, animal studies or studies with a non-fetal (neonatal, infant, child, or non-pregnant adult) phantom or a non-human (animal, digital, voxel, numerical, mathematical or computational) phantom were excluded from the analysis.

Screening

Potentially relevant articles were first identified based on whether their titles included the following keywords: ('fetal' OR 'phantom') AND ('MRI'). Articles with titles that made reference to any of the following exclusion criteria were excluded from abstract screening: non-English study, non-MRI study, a non-(fetal or phantom) study, an animal study or a study that used a non-fetal or a non-human phantom. The abstracts of the identified articles were then screened manually, and those not involving imaging phantom development or testing, or safety validation, accuracy, or motion-correction testing within a fetal MR study were excluded. The available full texts of the remaining articles were then reviewed, and only those satisfying all inclusion/exclusion criteria were included. Specifically, for the keyword title screening, alternative terms were identified prior to conducting the search, as shown in Table 1, and counted as equivalent terms. Duplicated search results were not removed.

Methodology review

To validate the accuracy and ensure the robustness of the described methodology, three equally trained research assistants conjointly followed the search strategy and repeated the literature search and screening.

Evaluation criteria

In our analysis, and based on the available literature, we are considering a fetal AMP for a given GA accurate if it:

1. Mimics the anatomy of the simulated body parts, providing a more realistic phantom for testing of MR pulse sequences [12].
2. Mimics the dielectric conductivity of the simulated tissues, so that it reproduces dielectric and chemical shift artifacts [30], correctly simulates the Specific Absorp-tion Rate (SAR) deposition of an imaging sequence, and thus, accurately models MR-induced heating effects [31].
3. Mimics the proton relaxation times of the simulated tissues, so that it correctly reproduces the contrast of a fetal MR image, thus guiding the selection of optimized parameters for a pulse sequence [32].
4. Simulates spontaneous gross fetal movement, and cardiovascular and respiratory motion, so that it mimics physiological MAs, allowing to create and test GA-specific motion-correction algorithms [12, 13].

Quantitative phantom analysis

The accuracy of the phantoms identified from the included studies was determined based on four equally weighted evaluation categories and eight subcategories, with each phantom being assigned up to a maximum of 12 merit points as follows:

Category 1: anatomical accuracy (3 points total)

Each phantom was awarded 1.5 points for anatomically accurate shape and 1.5 points for anatomically accurate size for the reported GA. Anatomical shape counted as accurate if the phantom was constructed directly from imaging scans or by exactly mimicking the anatomical profile of the simulated tissues using literature values. Anatomical size counted as accurate if the phantom was created based on anatomically accurate dimensions. If the shape was simplified or the dimensions scaled, 0.75 points were awarded. If the shape design or the dimensions were not discussed, no points were awarded.

Category 2: dielectric conductivity (3 points total)

Each phantom was awarded 3 points for mimicking the conductivity of all individual tissues being simulated for the specific GA. If only the average conductivity of the adult human body was simulated, 1.5 points were awarded. If only some but not all tissues were simulated, 1.5 points were awarded.

Category 3: relaxation times (3 points total)

Each phantom was awarded 3 points for mimicking the relaxation times of all individual tissues being simulated for the specific GA. If only some but not all tissues were simulated, then 1.5 points were awarded

Table 1 Alternate terminology in keyword title screening

Keyword	Alternative terms
Fetal	Fet[a], foet[a], in utero, intrauterine, prenatal, pregnant, gravid, womb, placenta, placental, amniotic fluid, umbilical, gestation, pelvimetry
MRI	Magnetic, magnetic resonance imaging, MR, MRS, SAR, NMR, T (as in Teslas), detection, surgical planning, or any imaging technique that uses or can use an MRI machine
Phantom	Model, motion-correction, distortion correction

[a]All variations of the root word with different suffixes were captured (e.g., fetus and fetoscopic)

Category 4: physiological motion (3 points total)

Each phantom was awarded 1 point each for mimicking fetal gross body movement, cardiovascular function, and respiratory motion with 100% accuracy. For fetal cardiovascular motion, simulating cardiac contraction and cardiovascular flow were awarded 0.5 points each for 100% accuracy. 100% motion accuracy was determined if the frequency of the simulated motion was within range of the expected fetal trunk, cardiovascular, or respiratory movement rates for the respective GA. If the simulated motion frequency was out of the expected range, the percent motion accuracy of the expected value was calculated and the awarded merit points were scaled accordingly. For example, the following calculation shows how points were awarded for a phantom with 100% (1) and sub-100% (2) cardiovascular motion accuracies:

1. 36 week cardiac phantom by Kording et al. [7].

   (a) Simulated motion frequency: 75–200 BPM for both cardiac contraction and cardiovascular flow.
   (b) Expected motion frequency at 36 weeks: 137 BPM [21].
   (c) Conclusion: 137 BPM is within the simulated range. Therefore, cardiac contraction and cardiovascular flow accuracy are both 100%.
   (d) Points awarded for simulating cardiovascular function: $0.5 \times 100\% + 0.5 \times 100\% = 1$ point.

2. 37 week blood vessel phantom by Jansz et al. [6].

   (a) Simulated motion frequency: no cardiac contraction with a maximum achievable cardiovascular flow frequency of 80 BPM.
   (b) Expected motion frequency at 37 weeks: 136 BPM [21].
   (c) Conclusion: 136 BPM is outside of the simulated range. Therefore, cardiovascular flow accuracy is: $(80\ \text{BPM}/136\ \text{BPM}) \times 100\% = 58.82\%$.
   (d) Points awarded for simulating cardiovascular function: $0.5 \times 0\% + 0.5 \times 58.82\% = 0.29$ points.

To the best of our knowledge, there have not been any comprehensive relaxometry and conductivity studies for fetal tissues for specific GAs. Thus, the accuracy of the reported relaxation times and conductivity values could not be verified and full points were awarded if these values were estimated based on theoretical calculations. These categories and merit points are summarized in Table 2.

Statistical analysis

Raw merit scores could not be used to provide a reliable review of the fetal MRI phantom field due to the nonhomogeneous point system. As a result, percentage accuracy was introduced to provide an unbiased parameter of the accuracy of each phantom. Percentage accuracy was calculated as the normalized points per evaluation category and reported as percentage values. This also allowed for a quantitative comparison between 3D printing versus conventional phantom synthesis methods, such as mold casting, use of household materials, and methods requiring only manual assembly. Using percentage accuracy also facilitated an unbiased comparison between the evaluation categories and subcategories to determine the status of the fetal MRI phantom field. This was complemented by a GA analysis to determine the trimester applicability for each phantom. Applicability was determined by the

Table 2 Phantom evaluation criteria point system

Evaluation category	Sub-category		Point(s) awarded
Anatomical accuracy	Same size as the simulated body part(s)	1	1.5
	Anatomically similar, but scaled		0.75
	Same shape as the simulated body part(s)	2	1.5
	Anatomically similar, but simplified		0.75
Dielectric conductivity	Simulates the specific conductivity of all simulated tissue(s)/body part(s)	3	3
	Simulates the average conductivity of the adult human body or, Simulates the specific conductivity of some but not all tissues within the phantom		1.5
Relaxation times	Simulates the specific proton relaxation times of all simulated body part(s)	4	3
	Simulates the specific relaxation times of some but not all tissues within the phantom		1.5
Physiological motion	Simulates spontaneous gross fetal movement in the gravid uterus	5	1–100% motion accuracy
	Simulates fetal cardiovascular function	6	0.5–100% contraction accuracy
		7	0.5–100% flow rate accuracy
	Simulates fetal respiratory breathing motion	8	1–100% motion accuracy

trimester which encompassed the majority of the reported GA range. However, if the reported GA range covered 50% or more of multiple trimesters, the phantom was recorded as applicable for each eligible trimester. The weekly ranges used were 0–13 weeks for the first trimester, 14–27 weeks for the second, and 28–40 weeks for the third, as per the guidelines provided by the American College of Obstetricians and Gynecologists [33]. Two-way unbalanced ANOVA followed by Tukey Honest Significant Difference tests were conducted for all analyses using Microsoft Excel 2016 (Microsoft, Seattle, USA) with an XLSTAT add-in (Addinsoft, Paris, France). $P < 0.05$ was considered statistically significant. To account for the non-normal data distributions within the synthesis method and evaluation category analyses, bootstrapping with 1999 resamples was conducted after the hypothesis testing [34]. The standard deviation of the resampled

means was then calculated to approximate the standard error of the mean (SEM) for each variable. The graphs and statistical results for these analyses are reported as bootstrapping mean $\pm$ SEM. While the reported evaluation category bootstrapping means were used to report the overall percentage accuracy per category, the sub-category results were reported as non-bootstrapping percent contributions as an approximation. Percent contribution was calculated as the normalized points per sub-category.

Results

Literature search results and methodology review

A total of 577 articles were identified according to the search criteria. A keyword search of their titles led to the removal
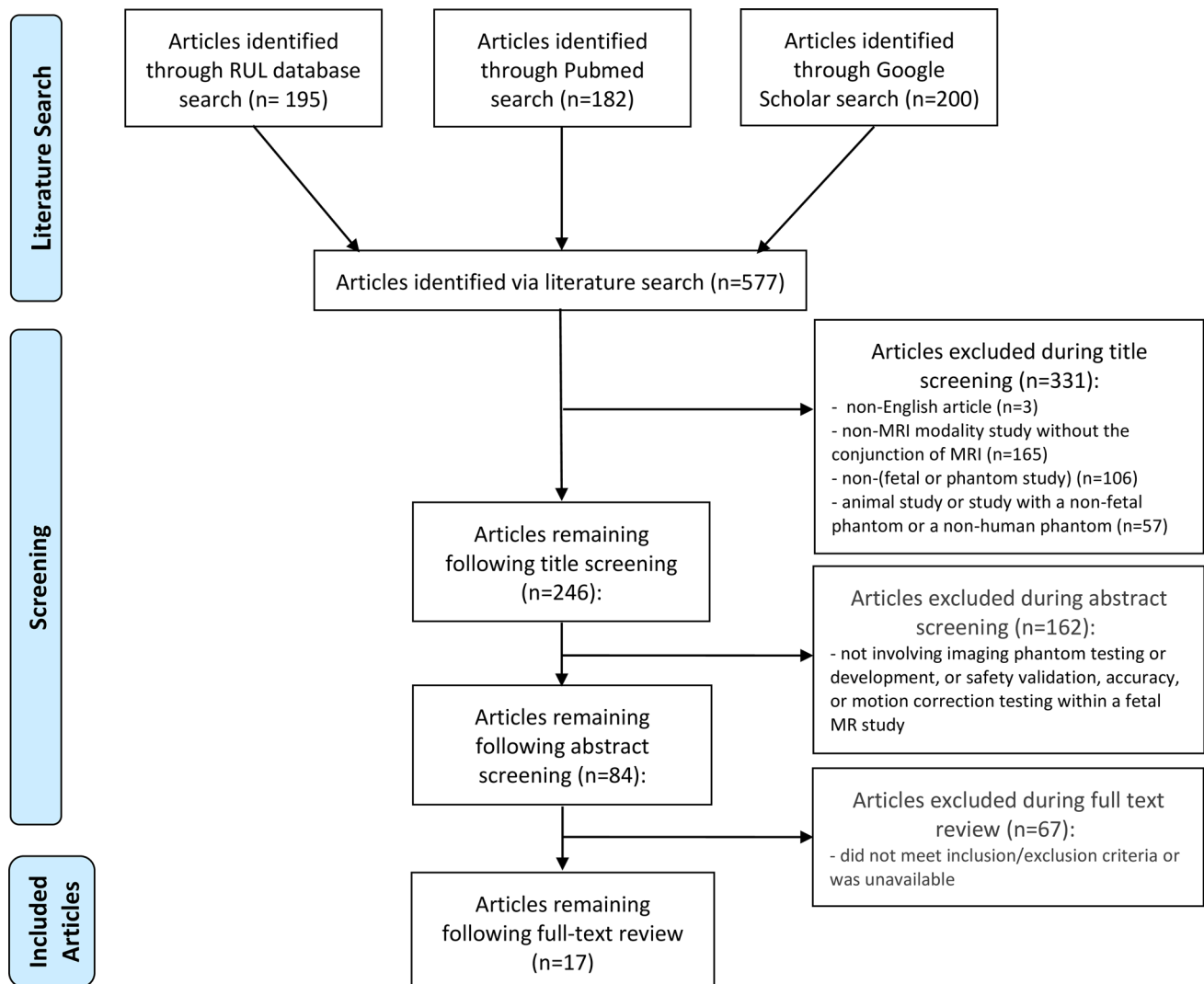

Fig. 1 Methodology and results of the narrative review

Table 3 Characteristics of the fetal MRI phantoms identified in the narrative review

Simulated body part	Citation	Simulated function	GA (weeks)	Manufacturing method	Phantom material	Simulated motion
Fetal gross body/gravid uterus	García-Polo et al. [8]	Relaxation times (T1/T2), dielectric properties	36	3D printing (direct)	Plastic (ABS-M30), rubber coating, epoxy resin, agar gel	No
	Victoria et al. [34]	SAR	20–30	Traditional	Saline bags, oil, water, cream-based salad dressing	No
	Spatz [35][a]	Relaxation times (T1/T2), dielectric properties	22	3D printing (direct)	Plastic (ABS-M30), rubber coating, epoxy resin, agar gel	No
	Chen et al. [36]	Dielectric properties	24	Traditional	Tissue-mimicking solution (NiSO4 6H2O, NaCl)	No
	Stark et al. [37]	Testing the accuracy of MR pelvimetry[b]	27–40	Traditional	Lucite, baby oil	No
Brain	Ferrazzi [38]	Testing the feasibility of fMRI	30–34	Traditional	Spherical flask, agarose gel	No
Lung	Büsing et al. [39]	Lung volume	14–32	Traditional (mold casting)	Gelatin, plastic sheaths	No
	Kehl et al. [40]	Lung volume	14–32	Traditional (mold casting)	Gelatin, plastic sheaths	No
Fetal body tissue	Victoria et al. [41]	Magnetic field interaction, MRI-related heating, artifacts	27–34	Traditional	Latex, gelled saline (NaCl, polyacrylic acid)	No
Heart	Kording et al. [7]	Cardiac motion	36	3D printing (indirect)	Silicone rubber, solenoid valves, hydro-motor	Yes
	Patel [15]	Cardiac motion	20–32	Traditional	Rubber balloon, acrylic pipe, polyvinyl carbonate (plastic), silicone tubes, silicone glue, vacuum pump	Yes
	Antoni et al. [16]	Fetal cardiac motion compensated by maternal breathing motion	9–40	Traditional	Linear actuator, UR5 robot, ultrasound damping plate, water tank, doppler ultrasound cardiotocography transducer, plastic heart phantom	Yes
Fetal blood vessel	Jansz et al. [6]	Flow pattern of blood	37	Traditional	Tube, servomotor, gear pump	Yes
	Portnoy [42]	Flow pattern of blood, relaxation times (T1/T2)	≥37	Traditional	Tube, programmable pump, MnCl2 and Gd solution	Yes
	Bidhult et al. [43]	Flow pattern of blood	28–40	Traditional	Tube, servo motor driven pump, flow rectifier, water tank	Yes
	Goolaub et al. [18]	Flow of blood	32–36	Traditional	Tube, computer-controlled pump	Yes
Placenta	Armstrong et al. [44]	Relaxation times (R2 = 1/T2)	14–23	Traditional	Test tube, agar gel, ferumoxytol	No

[a]The same construction methodology was used in the phantoms by Garcia-Polo et al. [8] and Spatz [35] as per communication with M. H. Spatz (July 2018) and Spatz [35] as per communication with M. H. Spatz (July 2018) and P. García-Polo (August 2018)

[b]Measurements of the female pelvis for obstetric purposes

Table 4 Summary of the identified phantoms

Simulated body part(s)	Brief description
Fetal gross body/gravid uterus	García-Polo et al. [8] constructed an anthropomorphic MR phantom of the gravid uterus with a 36-week old fetus (shown in Fig. 5). Each fetal and maternal body part was manually segmented, designed, and 3D-printed. Hollow compartments were filled with dielectrically accurate chemical compositions of agar-based tissue-mimicking gels
	Victoria et al. [35] constructed a fetal MRI phantom (shown in Fig. 6) with bottles of different consistencies wrapped with saline bags to imitate the fetus inside the amniotic sack. The fetal phantom was also placed inside an adult-sized phantom emulating the gravid uterus
	Spatz [36] used an anthropomorphic MR phantom of the gravid uterus with a 22-week old fetus (shown in Fig. 7). Similar to the phantom developed by García-Polo et al. [8], each fetal and maternal body part was manually segmented, designed, and 3D-printed. Hollow compartments were filled with dielectrically accurate chemical compositions of agar-based tissue-mimicking gels. This information was acquired through communication with M. H. Spatz (July 2018) and P. García-Polo (August 2018)
	Chen et al. [37] used a body-sized phantom to test a pregnant abdomen coil array. The phantom was filled with a solution that simulates the body's average dielectric properties
	Stark et al. [38] used an 11 cm-long lucite phantom filled with baby oil for testing the accuracy of MRI pelvimetry
Brain	Ferrazzi [39] constructed a fetal brain phantom using a circular flask filled with tissue-mimicking gels with nominally long T1 and T2 proton relaxation times, similar to those of fetal brain tissue
Lung	Büsing et al. [40] created 28 artificial fetal lung models from handmade plastic lung-shaped sheaths filled with 1–60 ml of gelatin (shown in Fig. 8)
	Kehl et al. [41] created 23 artificial fetal MRI lung models using the same methodology performed by Büsing et al. [40] (shown in Fig. 9)
Fetal body tissue	Victoria et al. [42] used an ASTM International plastic phantom filled with gelled saline to simulate human tissue. However, the phantom was specifically used to simulate fetal tissue when measuring the heating effects of the occlusive balloon used during fetoscopic tracheal occlusion
Heart	Kording et al. [7] built a fetal cardiac MRI phantom (shown in Fig. 10) from a 3D-printed mold of a CAD-designed biventricular heart model which was filled with silicone rubber. The phantom was placed in a sealed water container and connected to a hydro-motor controlled by an Arduino microcontroller. The phantom was able to simulate cardiac contraction and cardiovascular flow at 75–200 BPM
	Patel [15] constructed a dynamic heart phantom using a rubber water balloon placed inside a water-filled acrylic chamber. An Arduino control box, an external reservoir, and ventricular chambers were built to pump water in and out of the balloon at a frequency of 39–187 BPM simulating accurate cardiac contraction and cardiovascular flow
	Antoni et al. [16] constructed a fetal heart phantom (shown in Fig. 11) where cardiac contraction is simulated by a linear actuator moving the solid hemispherical phantom inside a water basin at a frequency range of 100–200 BPM. Maternal respiratory motion was also simulated by a robot inducing relative position between the phantom and the Doppler ultrasound cardiotocography transducer
Fetal blood vessel	Jansz et al. [6] developed a pulsatile flow MRI phantom that mimicked the movement of blood through a fetal blood vessel. The phantom used a computer-controlled servomotor and a programmable gear pump connected to a 10 mm inner diameter tube to create physiologically realistic flow patterns at a maximum achievable frequency of 80 BPM
	Portnoy [43] constructed a vessel flow phantom attached to a programmable pump with the capacity to generate a physiological flow pattern at a frequency of 150 BPM with a 10 mm inner diameter tube. $MnCl_2$-doped water and a Gd solution allowed for the simulation of umbilical cord blood relaxation times.
	Bidhult et al. [44] developed a pulsatile flow phantom that generated physiologically realistic flow patterns through a fetal blood vessel at a rate of 145 BPM. The phantom used a servo motor driven pump and a flow rectifier connected to a water tank by a 6 mm inner diameter tube
	Goolaub et al. [18] constructed a blood vessel phantom that generates constant flows (ranging from 10 to 60 mL/s). The computer-controlled pump was connected to a coiled 10 mm diameter tubing
Placenta	Armstrong et al. [45] constructed ten 50-ml test tubes with agar-based tissue-mimicking gels to simulate placental R2 relaxation times

Table 5 Merit points awarded for each identified phantom based on chosen evaluation criteria

| Simulated organ | Citation | Anatomy | | Conductivity (out of 3) | Relaxation times (out of 3) | Physiological motion | | | | Total points (out of 12) | Synthesis method |
		Size (out of 1.5)	Shape (out of 1.5)			Gross body (out of 1)	Cardiovascular		Respiratory (out of 1)		
							Contraction (out of 0.5)	Flow (out of 0.5)			
Fetal gross body/ gravid uterus	[8]	1.5	1.5	3	3	0	0	0	0	9	3D printing
	[35]	0	0.75	0	0	0	0	0	0	0.75	Traditional
	[36]	1.5	1.5	3	3	0	0	0	0	9	3D printing
	[37]	1.5	0.75	1.5	0	0	0	0	0	3.75	Traditional
	[38]	0	0	0	0	0	0	0	0	0	Traditional
Brain	[39]	0	0	0	0	0	0	0	0	0	Traditional
Lung	[40]	1.5	1.5	0	0	0	0	0	0	3	Traditional
	[41]	1.5	1.5	0	0	0	0	0	0	3	Traditional
Fetal body tissue	[42]	0	0	1.5	0	0	0	0	0	1.5	Traditional
Heart	[7]	0.75	0.75	0	0	0	0.5	0.5	0	2.5	3D printing
	[15]	0	0	0	0	0	0.5	0.5	0	1	Traditional
	[16]	0	0	0	0	0	0.5	0	0	0.5	Traditional
Fetal blood vessel	[6]	1.5	1.5	0	0	0	0	0.29	0	3.29	Traditional
	[43]	1.5	1.5	0	3	0	0	0.45	0	6.45	Traditional
	[44]	1.5	1.5	0	0	0	0	0.49	0	3.49	Traditional
	[18]	1.5	1.5	0	0	0	0	0	0	3	Traditional
Placenta	[45]	0	0	0	3	0	0	0	0	3	Traditional

of 331 articles. The abstracts of the remaining 246 articles were reviewed, of which 162 were excluded during abstract screening. Following a full-text review of the remaining 84 articles, 17 articles remained and were included in the narrative review paper. A flowchart of these search results is illustrated in Fig. 1 and the characteristics of the included studies and their corresponding fetal MRI phantoms are summarized in Table 3. A further summary of the identified phantoms is provided in Table 4 in the Appendix.

The repeated literature search confirmed the accuracy of the methodology; the same number of articles were identified and excluded in each screening step.

Quantitative phantom analysis

The results of the quantitative phantom analysis are shown in Table 5 and the percentage accuracy of each phantom per publication year is shown in Fig. 2. The statistical analyses for the synthesis method and evaluation category comparisons are shown in Figs. 3 and 4, respectively. The average overall accuracy for each phantom was $26 \pm 5\%$. The anatomical evaluation category had the highest percentage accuracy of $56 \pm 11\%$, while the least accurate was physiological motion with $7 \pm 3\%$ accuracy ($p = 0.0021$). Simulating anatomically correct shape and size equally contributed to the average anatomical accuracy (Fig. 4). The only source

Fig. 2 Percentage accuracy per publication year of fetal phantoms
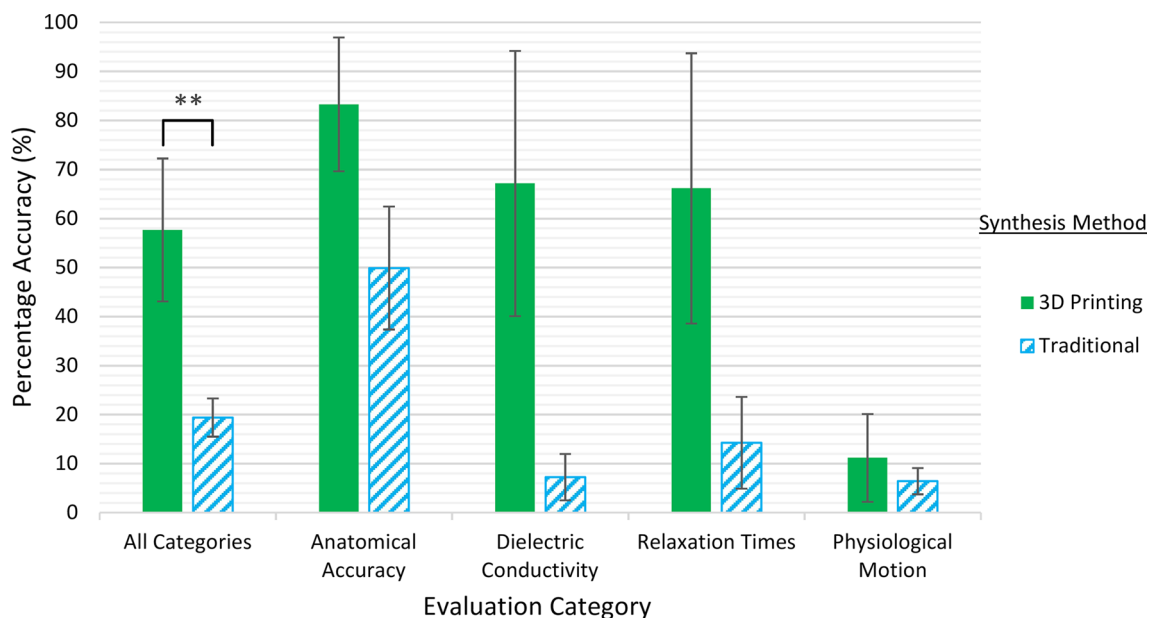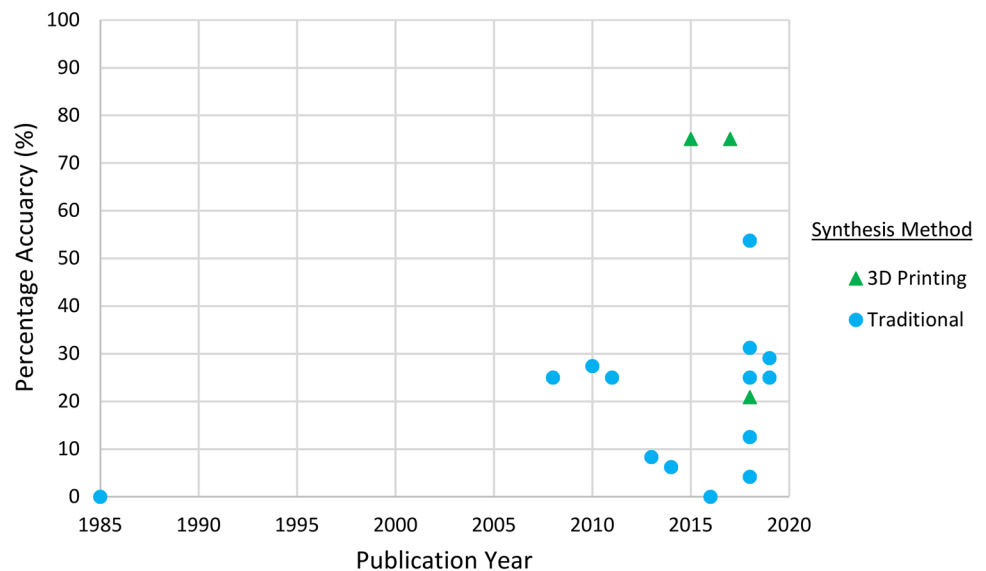
Fig. 3 Percentage accuracy comparison of 3D printing and traditional phantom synthesis methods per evaluation category (**$p < 0.01$)
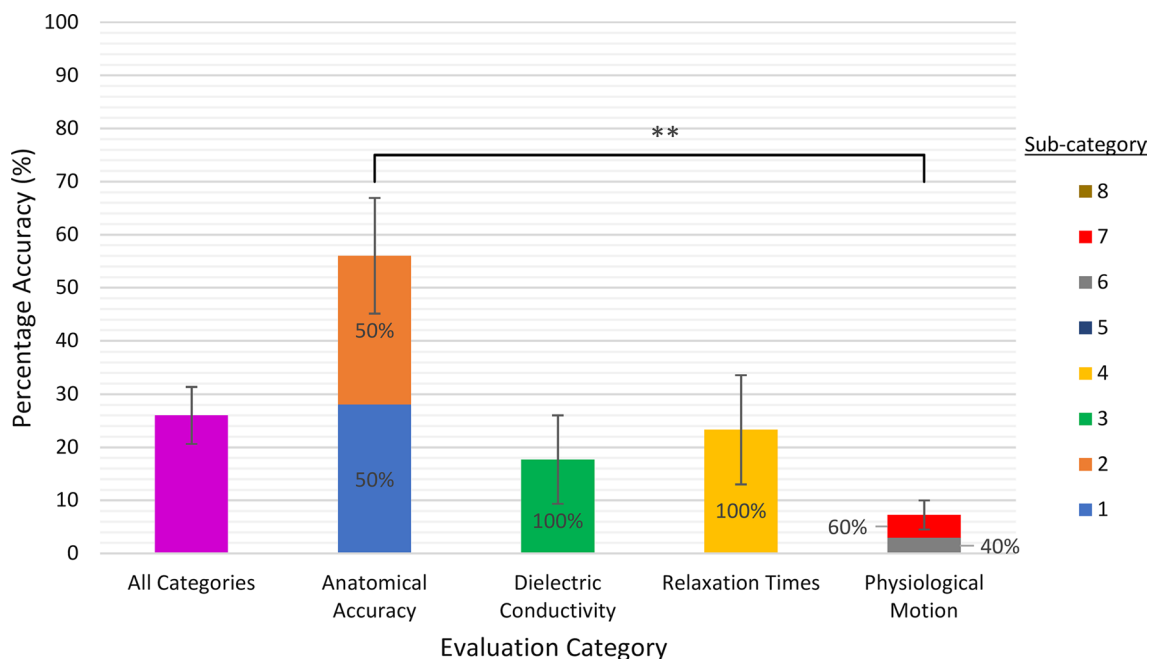
Fig. 4 Percentage accuracy per evaluation category, and percent contribution of each sub-category to the total percentage accuracy of each category (**$p < 0.01$)

Fig. 5 Various 3D-printed compartments of the anthropomorphic MR phantom of the gravid uterus developed by García-Polo et al. [8]
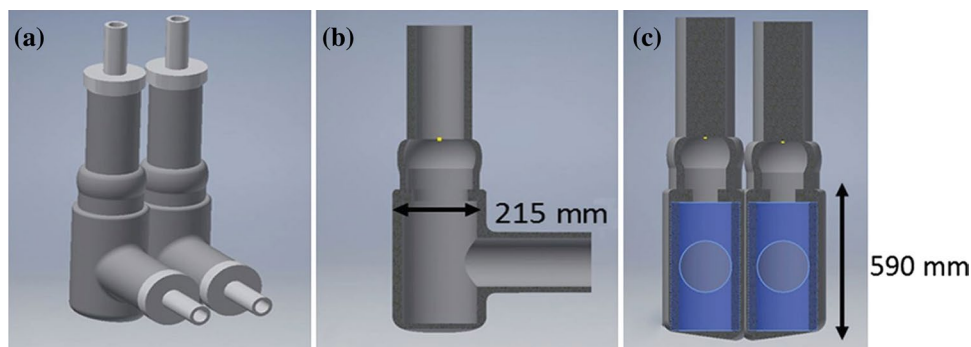

of motion simulation that our literature review found was that of cardiovascular function, with 60% of the accuracy arising from simulation of cardiovascular flow, as depicted in Fig. 4. However, none of the phantoms simulated gross body or respiratory motion. This demonstrates a significant gap in the literature since the identified phantoms were more likely to be anatomically correct than physiologically accurate. We also determined that 3D-printed phantoms had a higher average overall percentage accuracy ($58 \pm 15\%$) than traditionally constructed phantoms ($19 \pm 4\%$) ($p = 0.001$). While the power to draw a conclusion is limited because only three 3D-printed phantoms were identified, this indicates that using 3D printing tends to result in more accurate phantoms. Nonetheless, this limitation is expected since 3D printing is a relatively new technique that was first used for phantom manufacturing only in 2015. We also noted that the fetal MR phantoms identified were of either third trimester ($n = 10$) or

second trimester ($n = 8$), while there were no phantoms of first trimester.

Discussion

Overview of the fetal MRI phantom field

Based on our chosen evaluation criteria, the average percentage accuracy for the fetal phantoms identified in our literature search was only 26%, with the best phantom attaining a 75% accuracy. While the first published phantom was constructed in 1985, the majority of the identified phantoms were constructed between 2017 and 2019. This suggests that the use of fetal MR phantoms is increasing in popularity, reinforcing the need for a quantitative analysis of their accuracy to support and facilitate future development in the
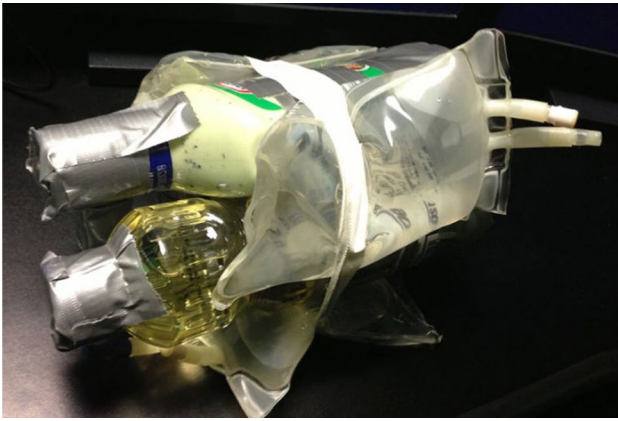
Fig. 6 A to-scale fetal MRI phantom constructed using saline bags, developed by Victoria et al [35]. Reprinted by permission from Springer Nature: Springer-Verlag. *Pediatr Radiol*. Fetal magnetic resonance imaging: jumping from 1.5 to 3 Tesla (preliminary experience). Victoria T, Jaramillo D, Roberts TPL, et al. ©2014
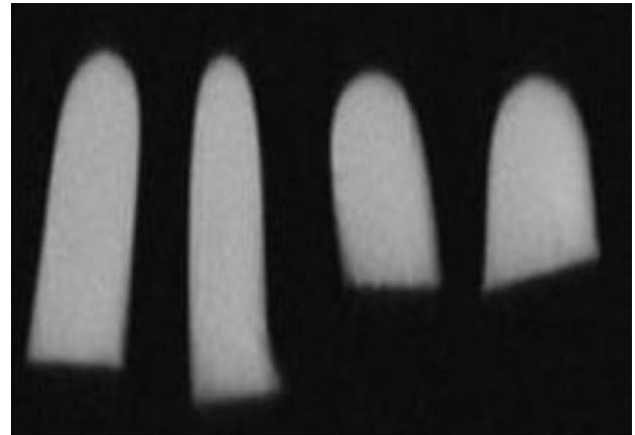
Fig. 8 4 –7 mL lung models developed by Büsing et al. [40] imaged with half-Fourier acquired single-shot turbo SE. Reproduced with permission from Büsing KA, Kilian AK, Schaible T, et al. Reliability and Validity of MR Image Lung Volume Measurement in Fetuses with Congenital Diaphragmatic Hernia and in Vitro Lung Models. *Radiology* 2008;246:553–561. Radiological Society of North America

**Fig. 7** Array coil posed on the anthropomorphic to-scale gravid uterus phantom used by Spatz [36]
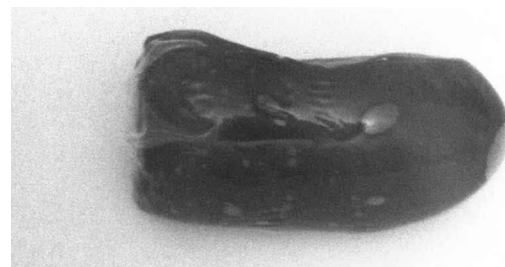
**Fig. 9** Hand-fashioned model mimicking the fetal lung developed by Kehl et al. [41]

field. Our analysis also determines that the majority of fetal phantoms are for second or third trimester.

The evaluation categories chosen to measure the accuracy of each phantom were equally weighted since the importance of each category is highly dependent on the phantom application. For example, anatomical accuracy is very important for the development of complex gravid uterus phantoms that are used as a proxy to human subjects to develop and test new fetal MRI pulse sequences [8, 36]. Simulating proton relaxation times is especially important when testing diagnostic sequences which monitor differences in relaxation times in diseased tissues, such as in the development of

R_2* mapping to diagnose ischemic placental disease [45]. Mimicking tissue conductivity is essential when developing phantoms to evaluate MRI-related heating effects [31], such as when assessing the safety of an occlusive balloon in MR-assisted fetoscopic tracheal occlusion [42]. Moreover, simulating accurate physiological motion is mandatory for the development of MRI triggering techniques for fetal cardiovascular MRI [16] or to validate metric optimized gating phase-contrast MR flow measurements [6, 44]. Given that all categories were equally weighted, the results suggest that the currently available fetal phantoms are significantly more likely to be anatomically correct than physiologically accurate. Namely, 8 out of the 17 identified phantoms simulated accurate shape and size for GA, while another 3 phantoms used a simplified and/or scaled model of the anatomy. Smaller phantoms require shorter image acquisition times than full-scale phantoms due to a smaller field of view and slice thickness; however, to achieve proportional image
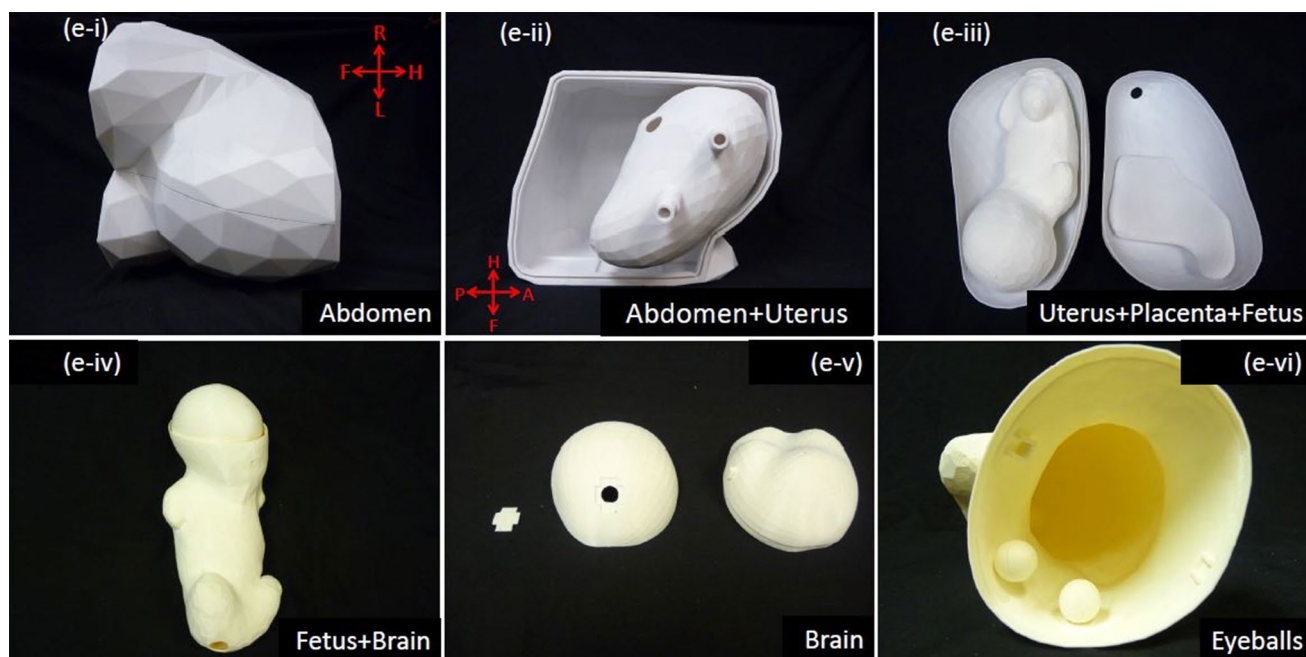
Fig. 10 The dimensions and setup of the fetal MRI biventricular heart phantom developed by Kording et al. [7]
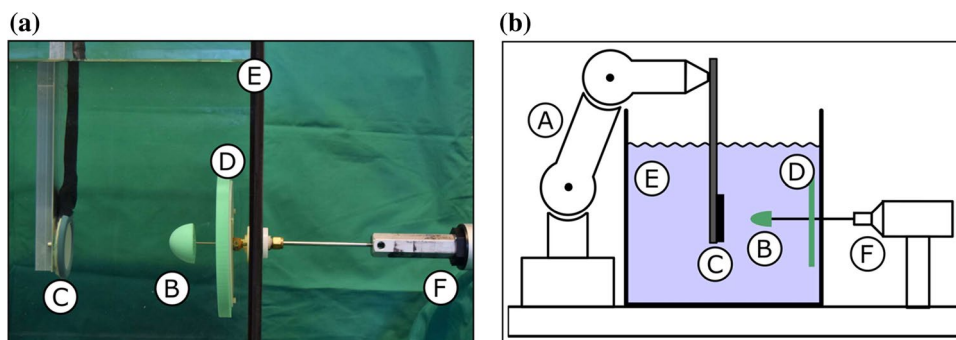
Fig. 11 Fetal cardiac phantom compensated with maternal respiratory motion developed by Antoni et al. [16]: the photograph (**a**) and schematic drawing (**b**) show a UR5 robot setup (A), heart phantom (B), CTG (C), US damping plate (D), tank (E) and linear joint (F) used to move the heart phantom. Reprinted by permission from Springer Nature. *Int J Comput Assist Radiol Surg*. Model checking for trigger loss detection during Doppler ultrasound-guided fetal cardiovascular MRI. Antoni S-T, Lehmann S, Neidhardt M, et al. ©2018

quality in small phantoms relative to full-scale phantoms, higher image resolution would be required [46]. Scaling or simplifying the anatomy also negatively affects which anatomical features can be distinguished in a phantom, making abnormality detection less accurate [47]. The importance of preserving both anatomically correct shape and size was evident as both subcategories equally contributed to the overall anatomical accuracy of each phantom. Thus, phantoms should be anatomically correct in terms of both size and shape to replicate the technical challenges of true human fetal MRI and permit more accurate validation and testing of new fetal MRI sequences [12]. Anatomical category

also had the highest percentage accuracy (56%) among all evaluation categories, reinforcing that anatomical accuracy is currently the most highly regarded criterion by fetal MR phantom developers.

The next evaluation categories with the highest percentage accuracy were relaxation times at 24%, followed by dielectric conductivity at 18%. While anatomical accuracy is usually the first consideration when constructing a phantom, to accurately test a new MR pulse sequence, correctly simulating the relaxation times of tissues is just as crucial. A difference in relaxation times can markedly affect the contrast of the image and the parameters needed for optimized

imaging protocol [18]. Refining a sequence using incorrect tissue relaxation times may result in poor image contrast when using the sequence on a human subject. Thus, having a phantom that mimics the tissue relaxation times can reduce the amount of time needed to test and refine an imaging sequence once it is translated into clinical applications. Similarly, dielectric conductivity must also be considered so that the phantom simulates the effects of the fetal tissue composition under MRI. Several image artifacts, such as central brightening [32], dielectric artifacts, and eddy current artifacts [30] depend on the conductivity of the material. Hence, simulating conductivity-related artifacts and the resulting image quality requires accurate simulation of material conductivity in the phantom. Moreover, accurate simulation of tissue conductivity permits evaluation of heating artifacts and calculations of the resulting SAR [31]. To the best of our knowledge, relaxometry of fetal or maternal tissues has only been quantified for the fetal brain [48], umbilical cord blood [43] and placenta [45], while conductivity has not been documented. As such, these values for other tissues can only be determined theoretically, as was done by García-Polo et al. [8] and Spatz [44]. Due to the lack of literature on this topic, the accuracy of the tissue relaxation times and conductivity simulated in the identified phantoms could not be evaluated. Since these values change throughout pregnancy due to the rapid growth, development and maturation of fetal tissues, a study that measures these values throughout pregnancy, and particularly between the age of viability (mid-second trimester) and term, would be valuable for facilitating accurate synthesis and design of fetal phantoms for specific GAs.

Very limited research has been conducted on replicating physiological motion in fetal MRI phantoms. Out of the 17 phantoms identified, only 7 were motion phantoms, of which only cardiovascular function was simulated. No phantom simulated spontaneous gross fetal body movement or fetal respiratory motion. Further in-depth research is needed to enable simultaneous accurate simulation of the different types of physiological motions in a fetal AMP. Such simulation would allow generating physiologically accurate MAs to test motion-correction approaches [13, 49] and the resulting SNR and contrast [49, 50]. Additionally, the refocusing RF pulses in Carr–Purcell–Meiboom–Gill (CPMG)-type sequences can cause tissue heating, which increase the need to monitor tissue temperature [1]. Accurately simulating motion would permit accurate MR gradient selection, which is of utmost importance to ensure fetal safety [1].

3D printing and traditional phantom manufacturing approaches

Our quantitative analyses also determined that phantoms constructed using 3D printing had a significantly higher overall percentage accuracy than phantoms constructed using other traditional methods, which indicates that 3D printing technology facilitates creating more accurate fetal MRI phantoms. While this conclusion is limited because of the small number of 3D-printed phantoms published to date, this new technique presents a promising development in the fetal MRI phantom field. Traditional phantoms, such as ones made through mold casting and those consisting of household materials and requiring only manual assembly, have several limitations. Most prominently, these phantoms cannot efficiently replicate the complex geometry of the human body [13, 51]. Specifically, the traditional techniques which were observed in the narrative review lacked the customizability necessary to replicate complex fetal anatomy. This was observed with 8 of the 14 traditional phantoms, which could not fully replicate the size and shape of the fetal and maternal anatomy [15, 16, 35, 37–39, 42, 45]. For example, Chen et al. [37] used a body-sized phantom, filled with a tissue-mimicking solution, to test a pregnant abdomen coil array. Although the phantom incorporated the approximate dimensions and even the rounded structure of the human torso, its estimated dimensions failed to simulate the topography of the pregnant abdomen. Another limitation is that the phantom was unable to simulate the internal anatomy of the gravid uterus due to its single-chamber structure. The remaining 6 traditionally constructed phantoms that were anatomically correct also had several disadvantages [6, 18, 40, 41, 43, 44]. For example, the lung phantoms produced by Kehl et al. [41] and Büsing et al. [40] were constructed from 'lung-shaped' sheaths filled with variable amounts of gelatin. Although the phantom procedure was simple and easy to follow, the manual construction method is susceptible to anatomical variability and subjectivity by the person constructing the phantoms. The use of 3D printing technology, which allows for direct printing of highly precise and complex structures from 3D fetal images, allows overcoming these issues, permitting more versatile, patient-specific, and relatively inexpensive prototyping of MRI phantoms [13, 51].

3D printing enables direct printing of the phantom or indirect printing of a mold, which is then filled with material which, when cured, is taken out of the mold [13, 52]. Direct 3D printing could also include printing a solid phantom or a hollow one which can then be filled with tissue-mimicking materials. Filippou [13] conducted a systematic review of 50 articles that developed 3D-printed phantoms for CT, MRI, PET, SPECT, ultrasonography and/or mammography

modalities. They determined that most of the 3D-printed phantoms had accurate dimensions [13]. Although 3D printers were shown to have an almost perfect anatomical accuracy [13], this accuracy depends on the prevalence of geometric distortions acquired during several manufacturing steps, including data acquisition, image processing, mesh refinement, and model manufacturing [13]. Key issues identified with the use of 3D printing include challenges with eliminating air bubbles in the tissue-mimicking solution, damaging the phantom when removing the support material, and using a sufficiently high imaging resolution which ultimately depends on the imaging modality [13]. Filippou [13] proposed several techniques for optimizing the manufacturing and the resulting anatomical accuracy, such as the use of a high-resolution CT scanner for data acquisition, adaptive slicing, and minimizing the amount of support material. Other challenges with 3D printing are related to simulating tissue anisotropy and strain-stiffness mechanical properties [51], which is essential for the accurate design of fetal cardiac and respiratory function in an AMP. Although the Young's modulus can be designed to be the same as that of the tissue being simulated, the creep tendency of polymeric materials results in a different stress–strain response under large deformations, making it challenging to maintain the desired strain-stiffness properties [51]. To overcome this issue, multi-material 3D printing technology can be used to seamlessly manipulate the mechanical properties of the phantom [51]. For example, dual-material 3D-printed metamaterials with microstructured reinforcement embedded in a soft polymeric matrix have been shown to mimic the strain-stiffening behaviour of soft tissues [53, 54].

Importantly, 3D printing can simplify the construction of anthropomorphic phantoms, which are anatomically accurate and simulate the specific fetal tissue conductivity and relaxation times. By this definition, only two anthropomorphic phantoms were identified in the review [8, 36]. Both gravid uterus phantoms consisted of directly 3D-printed hollow fetal and maternal organ compartments which were filled with agar-based tissue-mimicking gels. While this approach created the two most accurate phantoms, its disadvantage is the introduction of plastic boundaries in the 3D-printed compartments, which did not have the same dielectric and relaxation properties as the tissue-mimicking gels [8]. Ideally, one would be able to directly 3D print a complex fetal MRI phantom that possessed accurate dielectric and relaxation properties [52]. However, research in this field is very new and only a few studies to date have been able to manufacture 3D-printed MRI phantoms that produced a quantifiable MR signal; yet, none were for fetal MRI applications [52, 55].

Narrative review limitations

The main limitation of the current review is its very narrow inclusion criteria since only physical fetal MRI phantoms were evaluated. However, it is important to note that examining digital fetal MRI phantoms may be a valuable reference when building a physical model. In addition, the development of a fetal AMP might benefit from a broader review including neonatal phantoms as well as non-fetal AMPs. The effects of maternal motion can also be studied, as maternal motion from various causes (e.g. breathing, physiological bowel motion) has also been shown to cause MAs [16]. Furthermore, there is a growing interest in understanding maternal–fetal metabolic interactions [56], along with the respective anatomy, which would render a combined anthropomorphic MRI/MRS phantom a potentially useful tool for testing and developing multi-parametric pulse-sequence protocols [57].

Conclusion

With a fetal AMP, sequences and algorithms which correct for fetal motion without compromising image quality can be developed, resulting in improved prenatal diagnostic capabilities. Specifically, a fetal AMP would significantly decrease sequence development time and cost by permitting simultaneous multi-parametric optimization and avoiding the use of animal models or recruitment of pregnant patients. To survey the current fetal MRI phantom field, our comprehensive narrative review identified 17 fetal MRI phantoms. Each of the identified phantoms was then quantitatively analyzed based on their anatomical accuracy, dielectric conductivity, relaxation times, and physiological motion properties. The average overall accuracy among all phantoms was only 26% and phantoms were more likely to be anatomically than physiologically accurate. This indicates that extensive further research needs to be conducted to construct a fetal AMP which can simultaneously simulate accurate cardiovascular, respiratory, and gross body motion. Our quantitative analysis also revealed that 3D printing is superior to traditional methods since it facilitates the synthesis of overall more accurate phantoms. Yet, the most significant disadvantage of 3D printing phantoms is the introduction of plastic boundaries which do not simulate accurate conductivity and relaxation times. An additional challenge is the lack of comprehensive fetal relaxometry and conductivity studies. Therefore, future research should focus on developing GA-specific tissue-mimicking materials which can be directly 3D-printed. Finally, the next generation of fetal MRI phantoms should also use multi-material 3D printing with flexible solid materials to seamlessly control the mechanical properties of cardiovascular and respiratory soft tissues.

Author contributions Study conception and design, analysis and interpretation of data and critical revision: DS, MS. Acquisition of data: MS, EC, JC, SN, and BA. Drafting of manuscript: DS, MS, EC, and NW.

Compliance with ethical standards

Conflict of interest The authors declare that they have no conflict of interest.

References

1. Bulas D, Egloff A (2013) Benefits and risks of MRI in pregnancy. Semin Perinatol 37:301–304
2. Pugash D, Brugger PC, Bettelheim D, Prayer D (2008) Prenatal ultrasound and fetal MRI: the comparative value of each modality in prenatal diagnosis. Eur J Radiol 68:214–226
3. Biegon A (2014) Quantitative magnetic resonance imaging of the fetal brain in utero: methods and applications. World J Radiol 6:523–529
4. Gholipour A, Estroff JA, Warfield SK (2010) Robust super-resolution volume reconstruction from slice acquisitions: application to fetal brain MRI. IEEE Trans Med Imaging 29:1739–1758
5. Gholipour A, Estroff JA, Barnewolt CE, Robertson RL, Grant PE, Gagoski B, Warfield SK, Afacan O, Connolly SA, Neil JJ, Wolfberg A, Mulkern RV (2014) Fetal MRI: a technical update with educational aspirations. Concepts Magn Reson Part A 43A:237–266
6. Jansz MS, Seed M, van Amerom JFP, Wong D, Grosse-Wortmann L, Yoo S-J, Macgowan CK (2010) Metric optimized gating for fetal cardiac MRI. Magn Reson Med 64:1304–1314
7. Kording F, Schoennagel BP, de Sousa MT, Fehrs K, Adam G, Yamamura J, Ruprecht C (2018) Evaluation of a portable doppler ultrasound gating device for fetal cardiac MR imaging: initial results at 1.5T and 3T. Magn Reson Med Sci 17:308–317
8. García-Polo P, Gagoski B, Guerin B, Gale E, Adalsteinsson E, Grant PE, Wald LL (2015) An anthropomorphic MR phantom of the gravid abdomen including the uterus, placenta, fetus and fetal brain. In: ISMRM Annual Meeting, Abstract #1545
9. Serag A, Macnaught G, Denison FC, Reynolds RM, Semple SI, Boardman JP (2017) Histograms of oriented 3D gradients for fully automated fetal brain localization and robust motion correction in 3 T magnetic resonance images. Biomed Res Int 2017:1–8
10. van Amerom JFP, Lloyd DFA, Price AN, Kuklisova Murgasova M, Aljabar P, Malik SJ, Lohezic M, Rutherford MA, Pushparajah K, Razavi R, Hajnal JV (2018) Fetal cardiac cine imaging using highly accelerated dynamic MRI with retrospective motion correction and outlier rejection: fetal cardiac cine imaging using dynamic MRI. Magn Reson Med 79:327–338
11. Keraudren K, Kuklisova-Murgasova M, Kyriakopoulou V, Malamateniou C, Rutherford MA, Kainz B, Hajnal JV, Rueckert D (2014) Automated fetal brain segmentation from 2D MRI slices for motion correction. NeuroImage 101:633–643
12. Swailes NE, MacDonald ME, Frayne R (2011) Dynamic phantom with heart, lung, and blood motion for initial validation of MRI techniques. J Magn Reson Imaging 34:941–946
13. Filippou V, Tsoumpas C (2018) Recent advances on the development of phantoms using 3D printing for imaging with CT, MRI, PET, SPECT, and ultrasound. Med Phys 45:e740–e760
14. Cheung CL, Looi T, Drake J, Kim PCW (2012) Magnetic resonance imaging properties of multimodality anthropomorphic silicone rubber phantoms for validating surgical robots and image guided therapy systems. In: Holmes DR III, Wong KH (eds) Medical Imaging 2012: image-guided procedures, robotic interventions, and modeling. San Diego, USA
15. Patel M (2013) Design and development of a MRI and US compatible heart phantom. Master's Thesis, Hamburg University of Applied Sciences and University Medical Center Hamburg-Eppendorf
16. Antoni S-T, Lehmann S, Neidhardt M, Fehrs K, Ruprecht C, Kording F, Adam G, Schupp S, Schlaefer A (2018) Model checking for trigger loss detection during Doppler ultrasound-guided fetal cardiovascular MRI. Int J Comput Assist Radiol Surg 13:1755–1766
17. Hutter J, Christiaens DJ, Schneider T, Cordero-Grande L, Slator PJ, Deprez M, Price AN, Tournier J-D, Rutherford M, Hajnal JV (2018) Slice-level diffusion encoding for motion and distortion correction. Med Image Anal 48:214–229
18. Goolaub DS, Roy CW, Schrauben E, Sussman D, Marini D, Seed M, Macgowan CK (2018) Multidimensional fetal flow imaging with cardiovascular magnetic resonance: a feasibility study. J Cardiovasc Magn Reson 20:77
19. Malamateniou C, Malik SJ, Counsell SJ, Allsop JM, McGuinness AK, Hayat T, Broadhouse K, Nunes RG, Ederies AM, Hajnal JV, Rutherford MA (2013) Motion-compensation techniques in neonatal and fetal MR imaging. Am J Neuroradiol 34:1124–1136
20. Valenti O, Di Prima FAF, Renda E, Faraci M, Hyseni E, De Domenico R, Monte S, Giorgio E (2011) Fetal cardiac function during the first trimester of pregnancy. J Prenat Med 5:59–62
21. Snijders RJM, McLaren R, Nicolaides KH (1990) Computer-assisted analysis of fetal heart rate patterns at 20–41 weeks' gestation. Fetal Diagn Ther 5:79–83
22. Roberts AB, Little D, Cooper D, Campbell S (1979) Normal patterns of fetal activity in the third trimester. BJOG Int J Obstet Gynaecol 86:4–9
23. Cosmi EV, Anceschi MM, Cosmi E, Piazze JJ, La Torre R (2003) Ultrasonographic patterns of fetal breathing movements in normal pregnancy. Int J Gynecol Obstet 80:285–290
24. Natale R, Nasello-Paterson C, Connors G (1988) Patterns of fetal breathing activity in the human fetus at 24 to 28 weeks of gestation. Am J Obstet Gynecol 158:317–321
25. Ruano R, Joubin L, Aubry M-C, Thalabard J-C, Dommergues M, Dumez Y, Benachi A (2006) A nomogram of fetal lung volumes estimated by 3-dimensional ultrasonography using the rotational technique (virtual organ computer-aided analysis). J Ultrasound Med 25:701–709
26. Govindan RB, Vairavan S, Ulusar UD, Wilson JD, Mckelvey SS, Preissl H, Eswaran H (2011) A novel approach to track fetal movement using multi-sensor magnetocardiographic recordings. Ann Biomed Eng 39:964–972
27. Kuwata T, Matsubara S, Ohkusa T, Ohkuchi A, Izumi A, Watanabe T, Suzuki M (2008) Establishing a reference value for the frequency of fetal movements using modified 'count to 10' method: reference value for fetal movement. J Obstet Gynaecol Res 34:318–323
28. Kuwata T, Matsubara S, Ohkusa T, Yada Y, Suzuki M (2011) Decreased fetal movement prompts investigation of prenatal/neonatal nemaline myopathy: the possible merit of fetal movement count: fetal movement in fetal myopathy. J Obstet Gynaecol Res 37:921–925

29. Hayat TTA, Nihat A, Martinez-Biarge M, McGuinness A, Allsop JM, Hajnal JV, Rutherford MA (2011) Optimization and initial experience of a multisection balanced steady-state free precession cine sequence for the assessment of fetal behavior in utero. Am J Neuroradiol 32:331–338

30. Huang SY, Seethamraju RT, Patel P, Hahn PF, Kirsch JE, Guimaraes AR (2015) Body MR imaging: artifacts, k-Space, and solutions. Radiographics 35:1439–1460

31. Xin SX, Gu S, Carluccio G, Collins CM (2015) Consideration of the effects of intense tissue heating on the RF electromagnetic fields during MRI: simulations for MRgFUS in the hip. Phys Med Biol 60:301–307

32. Bernstein MA, Huston J, Ward HA (2006) Imaging artifacts at 3.0T. J Magn Reson Imaging 24:735–746

33. American College of Obstetricians and Gynecologists (2017) Methods for estimating the due date. committee Opinion No. 700. Obstet Gynecol 129:e150–e154

34. Carpenter J, Bithell J (2000) Bootstrap confidence intervals: when, which, what? A practical guide for medical statisticians. Stat Med 19:1141–1164

35. Victoria T, Jaramillo D, Roberts TPL, Zarnow D, Johnson AM, Delgado J, Rubesova E, Vossough A (2014) Fetal magnetic resonance imaging: jumping from 1.5 to 3 tesla (preliminary experience). Pediatr Radiol 44:376–386

36. Spatz MH (2017) A 64 channel 3T array coil for highly accelerated fetal imaging at 22 weeks of pregnancy. Master's Thesis, Massachusetts Institute of Technology

37. Chen Q, Xie G, Luo C, Yang X, Zhu J, Lee J, Su S, Liang D, Zhang X, Liu X, Li Y, Zheng H (2018) A dedicated 36-channel receive array for fetal MRI at 3 T. IEEE Trans Med Imaging 37:2290–2297

38. Stark DD, McCarthy SM, Filly RA, Parer JT, Hricak H, Callen PW (1985) Pelvimetry by magnetic resonance imaging. Am J Roentgenol 144:947–950

39. Ferrazzi G (2016) An exploration of methods for performing resting state fMRI in the human fetus. PhD Thesis, King's College London

40. Büsing KA, Kilian AK, Schaible T, Debus A, Weiss C, Neff KW (2008) Reliability and validity of MR image lung volume measurement in fetuses with congenital diaphragmatic hernia and in vitro lung models. Radiol 246:553–561

41. Kehl S, Zirulnik A, Debus A, Sütterlin M, Siemer J, Neff W (2011) In vitro models of the fetal lung: comparison of lung volume measurements with 3-dimensional sonography and magnetic resonance imaging. J Ultrasound Med 30:1085–1091

42. Victoria T, Johnson AM, Adzick NS, Hedrick HL, Shellock FG (2018) Evaluation of magnetic resonance imaging safety and imaging issues associated with the occlusion balloon used during fetoscopic endoluminal tracheal occlusion. Fetal Diagn Ther 44:179–183

43. Portnoy S (2018) Fetal Magnetic Resonance Oximetry. PhD Thesis, University of Toronto

44. Bidhult S, Töger J, Heiberg E, Carlsson M, Arheden H, Aletras AH, Hedström E (2019) Independent validation of metric optimized gating for fetal cardiovascular phase-contrast flow imaging. Magn Reson Med 81:495–503

45. Armstrong T, Liu D, Martin T, Masamed R, Janzen C, Wong C, Chanlaw T, Devaskar SU, Sung K, Wu HH (2019) 3D R2* mapping of the placenta during early gestation using free-breathing multiecho stack-of-radial MRI at 3T: free-Breathing Radial Placental R2* Mapping. J Magn Reson Imaging 49:291–303

46. Wargo CJ, Moore J, Gore JC (2013) A comparison and evaluation of reduced-FOV methods for multi-slice 7T human imaging. Magn Reson Imaging 31:1349–1359

47. He X, Frey EC, Links JM, Gilland KL, Segars WP, Tsui BMW (2004) A mathematical observer study for the evaluation and optimization of compensation methods for myocardial SPECT using a phantom population that realistically models patient variability. IEEE Trans Nucl Sci 51:218–224

48. Gagoski B, Ye H, Cauley S, Bhat H, Setsompop K, Chatnuntawech I, Martin A, Jiang Y, Griswold M, Adalsteinsson E, Grant PE, Wald L (2015) Magnetic resonance fingerprinting for fetal imaging at 3T—initial results. In: ISMRM Annual Meeting, Abstract #3429

49. Tavallaei MA, Johnson PM, Liu J, Drangova M (2015) Design and evaluation of an MRI-compatible linear motion stage. Med Phys 43:62–71

50. Freed M, de Zwart JA, Loud JT, El Khouli RH, Myers KJ, Greene MH, Duyn JH, Badano A (2011) An anthropomorphic phantom for quantitative evaluation of breast MRI: a phantom for quantitative evaluation of breast MRI. Med Phys 38:743–753

51. Wang K, Ho C-C, Zhang C, Wang B (2017) A review on the 3D printing of functional structures for medical phantoms and regenerated tissue and organ applications. Eng 3:653–662

52. Mitsouras D, Lee TC, Liacouras P, Ionita CN, Pietilla T, Maier SE, Mulkern RV (2017) Three-dimensional printing of MRI-visible phantoms and MR image-guided therapy simulation: 3D Printing of MRI-Visible Phantoms. Magn Reson Med 77:613–622

53. Wang K, Wu C, Qian Z, Zhang C, Wang B, Vannan MA (2016) Dual-material 3D printed metamaterials with tunable mechanical properties for patient-specific tissue-mimicking phantoms. Addit Manuf 12:31–37

54. Wang K, Zhao Y, Chang Y-H, Qian Z, Zhang C, Wang B, Vannan MA, Wang M-J (2016) Controlling the mechanical behavior of dual-material 3D printed meta-materials for patient-specific tissue-mimicking phantoms. Mater Des 90:704–712

55. In E, Walker E, Naguib HE (2017) Novel development of 3D printable UV-curable silicone for multimodal imaging phantom. Bioprinting 7:19–26

56. Feldt-Rasmussen U, Mathiesen ER (2011) Endocrine disorders in pregnancy: physiological and hormonal aspects of pregnancy. Best Pract Res Clin Endocrinol Metab 25:875–884

57. Song K-H, Kim S-Y, Lee D-W, Jung J-Y, Lee J-H, Baek H-M, Choe B-Y (2015) Design of a fused phantom for quantitative evaluation of brain metabolites and enhanced quality assurance testing for magnetic resonance imaging and spectroscopy. J Neurosci Methods 255:75–84